Surface Plasmon Optical Tweezers: Tunable Optical Manipulation in the Femtonewton Range

Maurizio Righini,[1] Giovanni Volpe,[1] Christian Girard,[2] Dmitri Petrov,[1,3] and Romain Quidant[1,3,*]

[1]*ICFO—Institut de Ciencies Fotoniques, Mediterranean Technology Park, 08860 Castelldefels (Barcelona), Spain*
[2]*CEMES, UPR-CNRS 8011, 29 rue Jeanne Marvig, 31055 Toulouse, France*
[3]*ICREA—Institució Catalana de Recerca i Estudis Avançats, 08010 Barcelona, Spain*

(Received 8 October 2007; revised manuscript received 10 March 2008; published 6 May 2008)

We present a quantitative analysis of 2D surface plasmon based optical tweezers able to trap microcolloids at a patterned metal surface under low laser intensity. Photonic force microscopy is used to assess the properties of surface plasmon traps, such as confinement and stiffness, revealing stable trapping with forces in the range of a few tens of femtonewtons. We also investigate the specificities of surface plasmon tweezers with respect to conventional 3D tweezers responsible for their selectivity to the trapped specimen's size. The accurate engineering of the trapping properties through the adjustment of the illumination parameters opens new perspectives in the realization of future optically driven on-a-chip devices.

DOI: 10.1103/PhysRevLett.100.186804 PACS numbers: 73.20.Mf, 87.80.Cc

Force fields originating from evanescent fields open new opportunities to integrate optical manipulation [1–4] in a coplanar geometry and to extend trapping to the subwavelength scale [5–7]. Within this scope, it was recently suggested to make use of surface plasmon (SP) fields bound to metal-dielectric interfaces. In addition to offering enhanced magnitude over conventional evanescent fields, SP fields are also expected to achieve further spatial confinement towards the nanoscale [8,9]. Enhanced optical forces on a single object exposed to the SP generated at a flat gold-water interface were first predicted [10] and lately experimentally probed using photonic force microscopy [11]. Experimental data have provided a force magnitude enhancement factor of about 40 that could be attributed to the plasmon resonance. A flat metal-dielectric interface under asymmetrical extended illumination leads to a homogeneous optical potential which attracts the bead toward the metal and pushes it along the incident in-plane k vector. The additional in-plane confinement required for trapping can be achieved by patterning the metal layer [9]. Lately, we have demonstrated that micrometer-sized gold pads microfabricated at the surface of a glass substrate and illuminated under total internal reflection enable trapping of single micrometer polymer beads [12]. In this configuration each pad supporting a SP resonance acts as a microlens leading to an intense local in-plane optical intensity gradient. This specificity can be exploited to achieve parallel trapping over nearly any predefined patterns contained within the illumination area.

Beyond these first qualitative observations, the development of SP tweezers for future on-a-chip devices requires a deeper understanding and a quantitative analysis of their properties. In this Letter, we investigate the main contributions to the trapping mechanism of SP tweezers and provide for the first time a study of their features, such as an optical potential profile and stiffness. We additionally demonstrate how the control of the illumination parameters enables selective trapping of particles with different sizes.

In our experiment, the trapping platform consists of isolated gold microdisks (4.8 μm diameter and 50 nm height) fabricated by e-beam lithography at the surface of a glass substrate [see Fig. 1(a)]. The illumination is performed under total internal reflection by a weakly focused (in-plane beam area 0.1 mm^2), linearly polarized laser beam at 710 nm. The incident power is fixed at 250 mW corresponding to an intensity $I \approx 2.5 \times 10^6$ W/m^2. Over the gold structures, a thin fluidic chamber containing a diluted solution of polystyrene (PS) microbeads is built. The dynamics of the beads is monitored with a

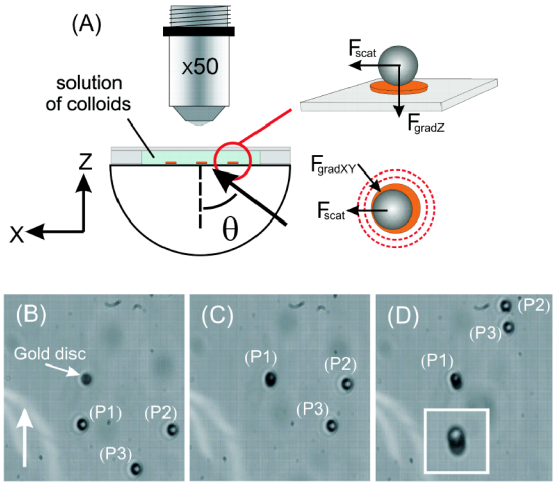

FIG. 1 (color online). (a) Sketch of the optical configuration. (b)–(d) Chronological frame sequence recorded for an incidence angle $\theta = 68°$ and p polarization showing the trapping of a 4.88 μm PS bead at a 4.8 μm gold pad. (P1), (P2), and (P3) locate three different beads, while the vertical arrow points along the incident in-plane k vector. A close up of the trapped bead (P1) is shown in inset of (d).

CCD camera using a long working distance objective lens. In Figs. 1(b)–1(d), a frame sequence of the trapping process of a 4.88 μm PS bead is shown when the incident polarization is p and the angle matches the plasmon angle $\theta_{SP} = 68°$ of a homogeneous gold-water interface. While the particles are guided at the glass/water interface along the incident in-plane k vector, pushed by the scattering force, particle (P1), passing close by the gold pad, gets efficiently trapped. Although the incident laser intensity is more than 2 orders of magnitude smaller than the minimum intensity typically required in conventional optical tweezers (OT) to trap such beads, stable trapping is observed over several tens of minutes.

Similarly to conventional OT, the trapping mechanism in SP tweezers relies on a suitable balance between scattering and gradient forces. Owing to the 2D geometry, both force components are here contained within the surface plane [Fig. 1(a)]. On the one hand, the scattering force pointing along the incident in-plane k vector is used as a motor for moving the particles across the trapping area. On the other hand, the intensity gradient of surface plasmon fields around the gold pad provides the in-plane gradient forces which tend to pull the bead towards the intensity maximum. In addition to optical gradients, coupling to SP leads to local heating of the metal and heat dissipation within the chamber. To minimize the contribution of thermal-induced dynamics, in addition to working with the low density of metal (isolated gold disk) we consider thin chamber thicknesses (< 20 μm) [13]. A major distinction over 3D OT comes from the dependency of both force contributions on the incident parameters such as the incident angle and polarization. Figure 2(a) gives the evolution with the incidence angle of the guiding velocity of 4.88 and 3.55 μm PS beads at a bare glass surface. In agreement with the first observations of Kawata and Sugiura [14], we find that the scattering force magnitude increases when decreasing θ. In a first approximation, this can be understood by the increase in the overlap of the bead volume with the evanescent tail of the incident field. The incident angle also controls the gradient force component when scanning across the pad SP band. As deduced from the reflectivity measurement of Fig. 2(b), the local field bound to the pad and thus the gradient force will be maximum at the plasmon resonance for $\theta_{SP} = 68°$. Consequently, the trapping properties of SP tweezers can be tuned by changing the balance between the two force components.

In order to appreciate the combined effect of θ on the trapping properties of a single pad, we plot in Fig. 2(c) the trapping probability for a 4.88 μm bead as a function of θ. In the experiment, a probability of 1 has been attributed for trapping times longer than 120 s. Applying this definition, three different regimes have been identified within the considered range of angles $64° \leq \theta \leq 69°$ under p polarization. While for $\theta \leq 65°$ the gradient restoring forces are weak because we stand out from the SP resonance and the scattering force is maximum, no trapping is achieved. Conversely, for $\theta \geq 67°$, the local intensity at the pad surface is maximum while the scattering force is minimum, leading to an efficient trapping of the bead. The scattering force is actually so weak in this case that significant trapping is also observed under s polarization without involving SP. Beyond this similarity in the trapping probability, the effect on the trapping potential introduced by the polarization state will be discussed later. Between these two limit cases, there is a transient regime where the ratio between both force contributions varies sharply with θ. Within this range, we have identified incidence conditions for which the bead is systematically stably trapped under p polarization while it quickly escapes under s polarization. In this last case, the uncertainty on the time to release the bead arises from its Brownian dynamics.

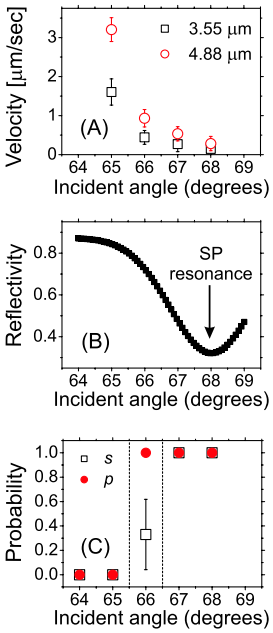

FIG. 2 (color online). (a) Evolution with the incident angle of the guiding velocity of 3.55 and 4.88 μm polystyrene beads at a glass/water interface. (b) Reflectivity curve of a flat 50-nm-thick gold film. (c) Evolution with the incident angle of the trapping probability of a 4.88 μm polystyrene bead near a 4.8 μm gold pad under both p and s polarization.

At this stage, one can get further insights into the specificities of SP traps by using photonic force microscopy [15,16]. This method, based on the tracking of the specimen dynamics, has been shown to be very well suited to fully characterize arbitrary force fields such as the torque produced by a vortex beam [17]. In a first step, a time series of the particle position under the combined effect of the trapping potential and the Brownian motion is acquired. In order to maximize the accuracy of the measurement, we increase the total recording time by reducing as much as possible the scattering force magnitude. This leads us to work with an incident angle $\theta = 68°$, where the contribu-

tion of the scattering force becomes weak while the restoring SP forces are maximum. The time scale of the bead motion is large enough so that its position can be reconstructed by video analysis with a frame rate of 15 fps [18]. Across the frames, the time evolution of the bead position can be retrieved by tracking its centroid. From the time series of the bead position, one can assess the shape of the potential energy function $U(l)$ ($l = X, Y$) by examining the histogram of the positions. The Boltzmann distribution describes the probability density $r(l) = e^{-U(l)/k_B T}/Z$, where Z is the partition function normalizing the probability density function, k_B the Boltzmann constant, and T the absolute temperature. This method permits us to check the assumption of a harmonic potential and when it is possible to proceed to the correlation [19] and the power spectral density analysis [20] of the position time series for the evaluation of the trap stiffness. This enables us to double-check the consistence of our results, verifying the uncorrelated nature of the motion along the X and the Y direction and ruling out any significant influence of external perturbations such as mechanical vibrations or drift.

Figure 3 gives the tracking diagram of a 3.55 μm PS bead (9 min acquisition time) for both p and s polarization. Under p polarization where the incident light efficiently couples to the SP mode of the gold pad, the potential is found to be confined to a small portion of the gold pad, shifted to a forward position with respect to its center. This feature is well corroborated by numerical simulations of the optical potential based on the Green dyadic method [21,22] (see Fig. 4). In order to save computer memory allocation, we have investigated a model system with dimensions 10 times smaller than the experimental ones. Such reduced dimensions, which generate tractable numerical self-consistent matrices compatible with available computer resources, appear sufficiently realistic to restitute qualitatively the main experimental features. Further quantitative comparison of the potential would require considering in the model the exact gold pad and bead sizes used in the experiment.

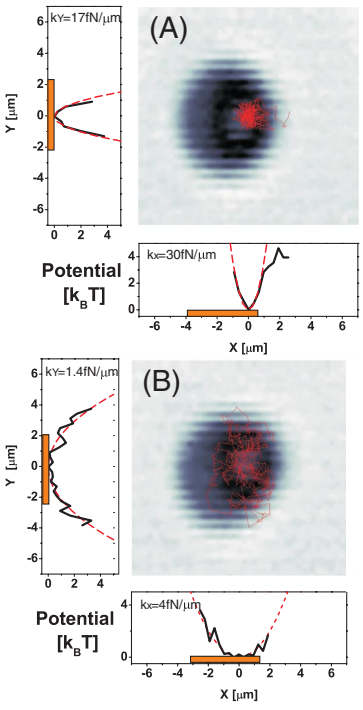

FIG. 3 (color online). Tracking diagram of a 3.55 μm PS bead for $\theta = 68°$ under both (a) p and (b) s polarization and the resulting trapping potential along the X and Y axis.

From the distribution of the bead position, the optical potential profile and the trap stiffness can be assessed along both the X and Y directions. While the potential is found to be very well approximated by a harmonic function along the Y axis, we observe, in good agreement with numerical calculations, an asymmetrical profile along the X axis, accredited to the asymmetry of the illumination. Despite the very weak incident laser intensity used in our experiment, the potential depth is found to be greater than $4k_B T$, where $k_B T$ is the thermal energy. The resulting trap stiffness are of about 30 fN μm^{-1} along X and 17 fN μm^{-1} along Y. These unprecedented features may open new opportunities to the study of force fields in the range of femtonewtons where other techniques do not apply.

The confinement and depth of the trap are found to drastically change when switching the incident polarization from p to s where no SP resonance is coupled in. The bead trajectory extends over a much bigger portion of the pad with a standard deviation around its equilibrium position 3 times greater along the X direction and 4 times along the Y axis. This observation, fairly well corroborated by the calculations of Fig. 4, arises from the delocalization of the near-field intensity above the gold pad for this polarization. The combination of the trap stretching with the decrease of the local field intensity magnitude leads to stiffnesses about 10 times weaker than under p polarization. We have also observed (not shown here for conciseness) that by controlling the incident linear polarization state one can achieve any intermediate potential between the two previous ex-

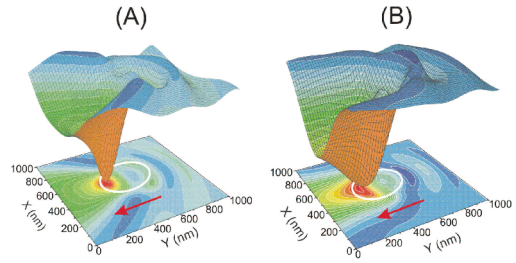

FIG. 4 (color online). Simulation of the optical potential maps computed for a 250 nm diameter polystyrene bead located 10 nm above a 450 nm diameter gold pad ($\theta = 68°$) under both (a) p polarization and (b) s polarization. The red arrow points along the incident k vector.

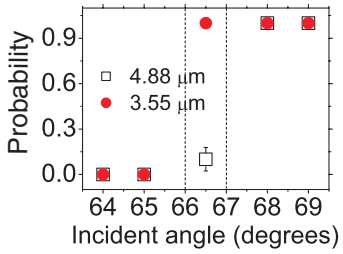

FIG. 5 (color online). Evolution with the incident angle of the trapping probability for both 3.55 and 4.88 μm PS beads under p polarization.

treme cases, rendering it possible to adjust the in-plane confinement of the SP trap.

Beyond the tunability of SP tweezers with the illumination parameters, one can additionally exploit the intrinsic dependence of both force components on the bead polarizability to control the trapping selectivity to the bead size observed in our prior work [12]. In order to illustrate this concept, we plot in Fig. 5 the trapping probability as a function of the incident angle (under p polarization) for both 3.55 and 4.88 μm beads. Although both bead sizes behave similarly for $\theta \leq 65°$ and $\theta \geq 68°$, between 66° and 67°, the smaller particle is efficiently trapped while the bigger one is quickly released. This may at first appear surprising, considering the corresponding trap features for each of the beads (see Table I). Lateral confinement and stiffness are indeed found to be comparable. However, it is here when the scattering contribution, 2 times stronger for the 4.88 μm bead [see Fig. 2(a)], makes the balance between scattering and restoring forces opposite for the two bead sizes. This feature, specific to SP tweezers, offers in practice the opportunity to control their selectivity to determined objects out of a mix by simply adjusting the incident angle.

Our study provides, to our knowledge, the first extensive quantitative analysis of SP tweezers formed at patterned metallic/dielectric interfaces. The accurate control of the different force contributions with the incident parameters such as incident angle and polarization draws the path towards a new generation of integrated devices where the transport and ultra gentle manipulation of small specimens could be efficiently driven with light.

TABLE I. Comparison of the stiffness along X and Y directions for two different PS bead sizes: 3.55 and 4.88 μm (p polarization, $\theta = 66.5°$).

	4.88 μm	3.55 μm
k_X	27 fN μm^{-1}	26 fN μm^{-1}
k_Y	22 fN μm^{-1}	17 fN μm^{-1}

This research was carried out with the financial support of the Spanish Ministry of Sciences through Grants No. TEC2007-60186, No. CSD2007-046-NanoLight.es, and No. NAN2004-09348-C04-02. The authors also thank María Ujué Gonzalez for fruitful discussions.

*romain.quidant@icfo.es

[1] A. Ashkin, Phys. Rev. Lett. **24**, 156 (1970).
[2] D. Grier, Nature (London) **424**, 810 (2003).
[3] K. C. Neuman and S. U. Block, Rev. Sci. Instrum. **75**, 2787 (2004).
[4] K. Dholakia and P. Reece, Nano Today **1**, 18 (2006).
[5] L. Novotny, R. X. Bian, and X. S. Xie, Phys. Rev. Lett. **79**, 645 (1997).
[6] P. Chaumet, A. Rahmani, and M. Nieto-Vesperinas, Phys. Rev. Lett. **88**, 123601 (2002).
[7] K. Okamoto and S. Kawata, Phys. Rev. Lett. **83**, 4534 (1999).
[8] H. Xu and M. Kall, Phys. Rev. Lett. **89**, 246802 (2002).
[9] R. Quidant, D. Petrov, and G. Badenes, Opt. Lett. **30**, 1009 (2005).
[10] Y. G. Song *et al.*, Opt. Commun. **198**, 7 (2001).
[11] G. Volpe, R. Quidant, G. Badenes, and D. Petrov, Phys. Rev. Lett. **96**, 238101 (2006).
[12] M. Righini, A. Zelenina, C. Girard, and R. Quidant, Nature Phys. **3**, 477 (2007).
[13] V. Garcés-Chávez, R. Quidant, P. J. Reece, G. Badenes, L. Torner, and K. Dholakia, Phys. Rev. B **73**, 085417 (2006).
[14] S. Kawata and T. Sugiura, Opt. Lett. **17**, 772 (1992).
[15] L. P. Ghislain and W. W. Webb, Opt. Lett. **18**, 1678 (1993).
[16] E. L. Florin, A. Pralle, J. K. H. Horber, and E. H. K. Stelzer, J. Struct. Biol. **119**, 202 (1997).
[17] G. Volpe and D. Petrov, Phys. Rev. Lett. **97**, 210603 (2006).
[18] C. Crocker and D. G. Grier, J. Colloid Interface Sci. **179**, 298 (1996).
[19] G. Volpe, G. Volpe, and D. Petrov, Phys. Rev. E **76**, 061118 (2007).
[20] K. Berg-Sorensen and H. Flyvbjerg, Rev. Sci. Instrum. **75**, 594 (2004).
[21] O. J. F. Martin, C. Girard, D. R. Smith, and S. Schulz, Phys. Rev. Lett. **82**, 315 (1999).
[22] C. Girard, Rep. Prog. Phys. **68**, 1883 (2005).